Plasmonic Nanobubbles as Tunable Theranostic Agents

E. Lukianova-Hleb, P.Constantinou, B.Danysh, D.S. Wagner, R.A.Drezek, J.H.Hafner, M.C. Farach-Carson,D.D.Carson and Dmitri Lapotko
*Rice University, Houston, TX, USA

ABSTRACT

Theranostic applications require coupling of diagnosis and therapy, a high degree of specificity and adaptability to delivery methods compatible with clinical practice. The tunable physical and biological effects of selective targeting and activation of plasmonic nanobubbles (PNB) were studied in a heterogeneous biological microenvironment of prostate cancer and stromal cells. All cells were targeted with conjugates of gold nanoparticles (NPs) through an antibody-receptor-endocytosis-nanocluster mechanism that produced NP clusters. The simultaneous pulsed optical activation of intracellular NP clusters at several wavelengths resulted in higher optical contrast and therapeutic selectivity of PNBs compared with those of gold nanoparticles alone. The developed mechanism was termed "rainbow plasmonic nanobubbles." The cellular effect of rainbow PNBs was tuned in situ in target cells, thus supporting a theranostic algorithm of prostate cancer cell detection and follow-up guided destruction without damage to collateral cells. The specificity and tunability of PNBs is promising for theranostic applications and we discuss a fiber optic platform that will capitalize on these features to bring theranostic tools to the clinic.

.

Keywords: theranostics, laser, gold nanoparticles, plasmonic nanobubbles, cancer

1 INTRODUCTION

Modern biomedical research and clinical practice have several principal challenges. The first barrier in current clinical practice is the separation of diagnosis, therapy and therapy guidance into three independent stages. This both impedes treatment procedures and reduces their accuracy. Theranostics was recently introduced as a concept of the combined diagnosis and treatment. Its successful realization will result in a significant improvement in both rapidity and precision in medical practice. The second limitation is the low sensitivity and specificity of current diagnostics and therapeutics that often cannot selectively identify and treat disease-specific cells and thus cannot support early-stage diagnosis and treatment. Being able to detect and treat disease selectively at cell level will result in earlier interventions and far higher treatment success rates. Current cellular probes do not provide true cell theranostics due to the limited tunability of their functions in the cells.

The biomedical applications of plasmonic nanoparticles (NPs) use their optical scattering properties for imaging and diagnostics, and their photothermal properties for various types of therapies through the generation of heat, bubbles and acoustic waves [1-5]. The specificity and sensitivity of imaging and diagnostics, as well as the selectivity and efficacy of the therapeutic methods, depend upon the selectivity of NP delivery and activation within their targets, typically diseased cells or tissues. The main limitation of various nanoprobes is the limited (or nonexistent) tunability of their function in a cell. We hypothesized that a further improvement in the selectivity and tunability of NP-based imaging, diagnosis, and therapy, and the unification of these steps into one theranostic procedure could be achieved with the simultaneous activation of the several different and co-locolized plasmon resonances in one NP cluster, and through the generation of tunable localized PNBs. Our current work is focused on the experimental evaluation of this hypothesis for gold NPs and associated PNBs. Below we report the experimental results for a new selective mechanism of PNB generation around clusters of gold NPs, and the evaluation of the developed mechanism at cell level for the theranostics of prostate cancer cells growing amidst normal stroma.

2 MATERIALS AND METHODS

The generation of a vapor bubble around a plasmonic NP (Figure 1A) requires a specific threshold of the fluence of the laser pulse. When the threshold is exceeded, the optical energy is converted in the NP by the mechanism of plasmon resonance into a sufficient amount of thermal energy that is rapidly transferred to the NP nano-environment, evaporates this nano-environment, and provides the expansion of the vapor into the nanobubble. The clustering of plasmonic NPs was shown to reduce the PNB generation threshold [6,7].

The described mechanism employs one plasmon resonance as the source of heat. We expanded this approach into a principally new mechanism that employs the simultaneous effect of several different plasmon resonances in one NP cluster. This was realized through using two different types of plasmonic (gold) NPs, rods and spheres, and their clustering through collective endocytosis (Figure 1B). If this multi-NP cluster is irradiated with one laser pulse at sub-threshold fluence (below the PNB threshold for clusters of a similar size though built of only one type of NP) there will be no bubble (Figure 1C). However, if we irradiate this multi-NP cluster with two simultaneous pulses at two different wavelengths (matching the plasmon

resonances of the NPs), their cumulative thermal effect will exceed the PNB threshold and will result in a PNB (Figure 1C). This "rainbow" mechanism is principally different from the standard one in the following ways:

1. A single source of optical energy (a laser pulse at a single wavelength) is replaced by several sources (several pulses of different wavelengths), while the fluence of each pulse is reduced below the PNB generation threshold for each corresponding NP type. In such cases, the simultaneous exposure of the mono-NP cluster or the single pulse exposure of the mono- or multi-NP cluster will not generate a PNB, because the thermal output in both cases will be insufficient, and only the simultaneous excitation of the multi-NP cluster will cause the bubble.
2. A reduced fluence of laser pulses results in a reduced initial temperature of individual corresponding NPs compared with the case of a single pulse excitation. The simultaneous heating of closely packed different NPs results in a rapid fusion (superposition) of their thermal fields into one joint thermal field surrounding the NP cluster. This thermal field acts as the energy source for the vapor bubble formation and expansion, and, compared with the single plasmon resonance case, the thermal load on the NPs is reduced, thus better protecting them from melting and enabling multiple activations.
3. The independent control of the fluence of each laser pulse allows us to optimize the excitation of the multi-NP cluster for maximal selectivity of PNB generation, whereas excitation with a single pulse does not offer this opportunity.

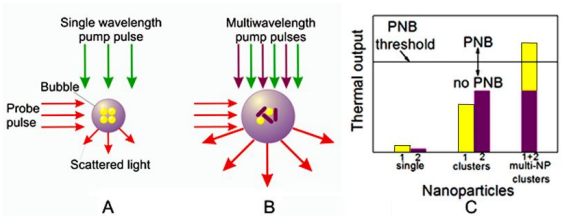

Figure 1. Principle of optical generation and detection of (A) standard PNB generated with single laser pulse around mono-NP cluster and (B) rainbow PNB generated with several laser pulses (shown with green and purple arrows) and multi-NP cluster (yellow and purple NPs with different plasmon resonances), (C) thermal outputs of single NPs, mono-NP clusters and multi-NP cluster under identical optical excitation with two laser pulses (as in case (B)): only the synergistic effect of two simultaneous plasmon resonances in one NP cluster deliver the thermal energy sufficient for PNB generation. Red arrows in (A) and (B) show PNB detection through optical scattering of an additional probe laser beam.

Optical generation and detection of the PNBs was performed with a previously developed photothermal laser microscope [8] equipped with a dual pulsed laser (STH-01, Standa Ltd, Vilnius, Lithuania): each pulse 0.5 ns, the wavelength of 532 nm (matching plasmon resonances of gold spheres of 60 nm) and tunable near-infrared (matching plasmon resonances of gold nanorods and nanoshells that were employed). Three types of gold NPs were used to form the multi-NP clusters: gold spheres (50 and 60 nm), rods (25x75 nm) and shells (52 nm). The optical detection of PNBs was realized in two parallel modes: time-resolved scattering imaging and time response [8]. The PNBs were quantified by measuring their lifetime, bubble generation threshold fluence and the pixel amplitude of their scattering images.

3 RESULTS

We studied the process of the generation of PNBs in individual cells in a co-culture of living bone metastatic prostate cancer (C4-2B) and human bone marrow stromal (HS-5) cells *in vitro* under the following conditions:

1. The initial targeting of the cells with gold NPs was supported by using a combination of the two different antibodies that were conjugated to specific different gold NPs. We applied prostate cancer-specific gold conjugates of NSP with PSMA (prostate specific membrane antigen) and gold NS conjugated with C225 (Erbitux, the antibody raised against human EGF receptor) that is tumor-associated, although it is less specific to prostate cancer cells than PSMA. The specificity and efficacy of PSMA-based targeting was independently verified with fluorescent confocal microscopy (LSM-710, Zeiss) of C4-2B and HS-5 cells that were identically treated with the conjugate of fluorescent dye with PSMA, AlexaFluor488-PSMA. This step did not provide absolute specificity of the targeting and, therefore, we applied the next targeting step.
2. The clustering of the membrane-accumulated NPs was provided by their endocytosis and subsequent aggregation in endosomal compartments in the cytoplasm. This process was monitored in C4-2B and HS-5 cells that were incubated with gold NPs by using the reflecting mode of the confocal microscope with a 633 nm laser. The size of NP clusters was analyzed through the image pixel amplitude of the scattering images of the NP clusters in cells. According to this metrics, the C4-2B cells formed much bigger clusters of NPs than those in HS-5 cells.

Next, living cells were individually exposed to single laser pulses of a specific wavelength and fluence and to pairs of laser pulses. PNBs were detected and quantified through their responses and time-resolved scattering images. Thus we obtained the probability of PNB generation, lifetime and scattering image amplitude. The cell was exposed to laser pulses at 532 nm@10 mJ/cm^2, 787 nm@8 mJ/cm^2 and to the simultaneous pair of these pulses. The PNB lifetimes and the probabilities of their generation were plotted as shown in the diagram (Figure 2). Almost no PNBs were generated in cells in single-pulse mode (Figure 2). However, the dual-pulse mode returned PNBs with a lifetime above 100 ns. This was achieved without increasing the fluence of laser pulses (that was, in this case,

within the FDA-approved safe limit, 20 mJ/cm^2) and through the rainbow mechanism of PNB generation. To achieve a similar PNB lifetime in single pulse mode in the same cells, we had to increase the fluence of the 532 nm pulse to 27 mJ/cm^2, a level higher than the summarized fluence of 532 nm and 675 nm pulses (18 mJ/cm^2) and also higher than the FDA-approved safety limit. The obtained lifetimes of PNBs (Figure 2) indicated a significant difference between the single pulse and dual pulse (rainbow) excitation modes. The lifetime of the rainbow PNBs was one to two orders of magnitude higher than the lifetimes of PNBs under a single pulse excitation. The latter were mainly not generated at all under the reduced level of laser fluences.

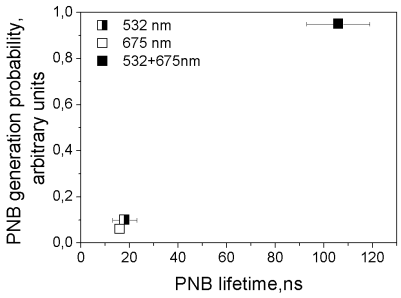

Figure 2: PNB lifetime-probability of generation diagrams obtained for prostate cancer cells (C4-2B) that were treated with hollow gold shells 52 nm and were exposed to single and paired laser pulses (532 nm@10 mJ/cm^2 and 675 nm@8 mJ/cm^2): half right square – single pulse 532 nm, hollow square – single 675 nm pulse, solid square - pair of laser pulses at 532 nm and 675 nm.

The diagnostic specificity and sensitivity of PNBs were evaluated by comparing the brightness and optical contrast of rainbow PNBs with those of gold NPs (scattering) and AlexaFluor488 label (PSMA-specific fluorescence) (Figure 3). We applied the reduced fluence (532 nm@10 mJ/cm^2 and 787 nm@12 mJ/cm^2) in order to generate relatively small, non-invasive PNBs with a lifetime below 100 ns (that had previously been found to be the threshold for transition from non-invasive to ablative bubbles [9,10]). The viability of each individual cell was monitored by measuring the level of fluorescence of specific vital dyes that leak out from the damaged cell (PNB-induced cell damage was shown to have a disruptive mechanical nature). We fluorescently labeled stromal (HS-5) and prostate cancer cells (C4-2B) with calcein vital dyes of red (cancer) and green (stromal) colors and mixed them in the proportion HS-5:C4-2B of 5:1 (Figure 3A). The brightness of the PNBs in cancer C4-2B cells (measured as the pixel image amplitude of the PNB, Figure 3F) was found to be 71 times higher than that for stromal cells (Figure 3H). Such an optical contrast exceeded the optical contrast of the fluorescent labels (that were targeted to C4-2B and HS-5 cells using the same prostate cancer-specific PSMA antibody, see Figure 3B, D) by 31 times. The optical contrast (measured as a ratio of the fluorescent image amplitudes for C4-2B to HS-5) of fluorescent imaging for cancer versus stromal cells was 2.3 (Figure 3B, D). Such a high contrast of PNB imaging was achieved due to their threshold mechanism: no PNBs were generated in HS-5 cells (Figure 3H), and their images were formed by the optical scattering by gold NPs that did not produce PNBs.

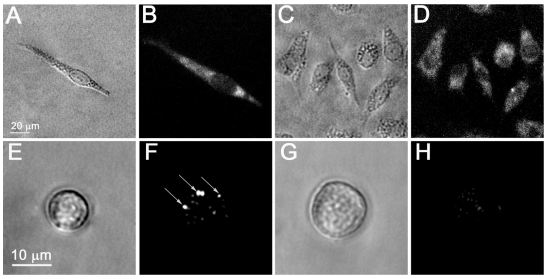

Figure 3: Microscopy images of living cells: bright field (A,C,E,G), time-resolved optical scattering (B,F) and fluorescent (AlexaFluor488 conjugated to PSMA antibody, D,H) images of prostate cancer C4-2B (A,B,E,F) and stromal HS-5 (C,D,G,H) cells; (F) and (H) – time-resolved scattering images of the cells presented in (E) and (G), respectively, that were exposed to the pair of laser pulses at 532 nm and 787 nm: image (F) shows the rainbow PNB in a C4-2B cell while the image (H) shows no PNB and only the scattering by residual gold NPs in HS-5 cell.

The above results were achieved with a single exposure of each cell to the pair of pump laser pulses. As can be seen from Figure 4B, the PNBs did not cause detectible changes in the level of Calcein AM fluorescence. Therefore, this diagnostic stage of PNB treatment can be considered as non-invasive for all cells being treated - target prostate cancer C4-2B cells and non-specific stromal HS-5 cells.

The next, therapeutic, stage of PNB treatment was realized by increasing the energy of the pump laser pulses to the level that provided the PNB lifetime well above cell damage level (i.e. longer than 100 ns). We evaluated the rainbow PNBs for the selective ablation of cancer cells surrounded by non-cancer stromal cells (a typical cancer microenvironment described above for the diagnostic stage). Next, we treated the mixture of cells with the two gold conjugates and with two laser pulses, 532 nm@16 mJ/cm^2 and 787 nm@19 mJ/cm^2. The sample was scanned through the laser beam and each cell was identified according to its fluorescence (Figure 4B), and was then exposed to a single pair of laser pulses (Figure 4C). Based upon the PNB generation probabilities and lifetimes, the stable PNBs were generated under the rainbow mechanism and in cancer cells only. PNBs were also observed on occasion in stromal cells, but their probability was below 20%, and their size was small compared to the size of cancer-cell generated PNBs. This latter result inspired an additional test: because cell damage by a PNB depends upon its size (lifetime [9,10]), we monitored and compared

the vital fluorescence of PNB treated cancerous and stromal cells.

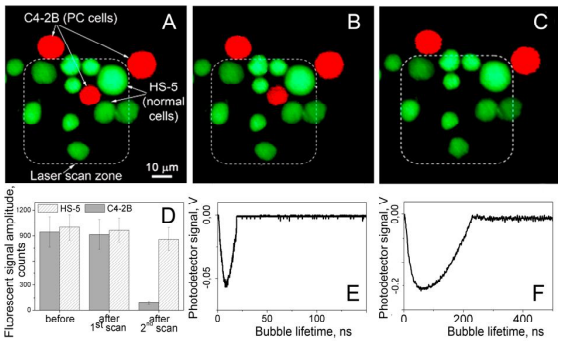

Figure 4: Fluorescent images of the mixture of prostate cancer C4-2B (red) and stromal HS-5 (green) cells: (A) before, (B) after the first scan and (C) 60 s after the second scan, exposure to the pair of laser pulses (532 nm and 787 nm) that selectively generated cell damaging PNBs causing fading of red fluorescence due to leaking of red calcein out through the disrupted membrane. Dashed line shows the area that was exposed to the laser pulses. D – cell population averaged fluorescent signal amplitudes for C4-2B and HS-5 cells before and after treatment with laser pulses. E and F – the time responses of PNBs in C4-2B cell obtained during the first and the second scans.

Within the area irradiated with laser pulses (shown within a dashed line in Figure 4B,C) we discovered that only the cancer cell was damaged. The vital dye stays in the cell with an intact membrane and quickly leaks out of the cell with a compromised membrane. The damage (ablation) of the cancer cell in the center (observed as the loss of the red fluorescence) was in line with the increased size (lifetime) of the PNBs generated specifically in C4-2B cells, and with the mechanical nature of cell damage that is associated with the disruption of the cellular structures including the plasma membrane. This final test clearly demonstrates the selectivity of the rainbow PNBs that were generated locally in a single specific (cancer) cell and were not generated in the surrounding stromal cells (or were generated in such cells with a probability and size that prevented their damage). While the vital fluorescent images in Figure 4B,C demonstrate the potential of rainbow PNBs for selective therapy, the optical scattering of these PNBs has a high diagnostic potential.

We conclude that the suggested method of cell theranostics with "rainbow plasmonic nanobubbles" demonstrates the following advantages over other methods of photothermal excitation of plasmonic NPs and PNBs:

1. The synergistic excitation of several plasmon resonances in the clusters of gold (plasmonic) NPs significantly improves the efficacy of the generation of plasmonic nanobubbles and is referred to as "rainbow plasmonic nanobubbles".
2. Rainbow plasmonic nanobubbles can be generated under reduced fluences of the excitation laser pulses that are below the PNB generation threshold for single NPs and for clusters consisting of only one type of NPs.
3. The mechanism of rainbow plasmonic nanobubbles significantly improves the selectivity of bubble generation in specific target cancer cells compared to non-specific stromal (non-cancer) cells and can therefore provide the cell level selectivity needed for diagnosis and therapy.
4. Rainbow plasmonic nanobubbles are less sensitive to the NP cluster content than the plasmonic nanobubbles generated around mono-NP clusters whose content can vary in cells due to the heterogeneous nature of NP uptake by living cells.
5. PNBs demonstrates the tunability of their function in individual cells, thus performing the diagnosis and guided treatment that can be united into a single connected theranostic procedure.

As a result rainbow plasmonic nanobubbles can be considered as a novel platform for developing cell level diagnostic, therapeutic and theranostic solutions for treating various pathologies such as prostate cancer.

REFERENCES

[1] Hirsch LR, Gobin AM, Lowery AR, et al. Ann Biomed Eng 34, 15, 2006.

[2] Cherukuri P, Glazer ES, Curley SA. Adv Drug Deliv Rev 62, 339, 2010.

[3] Kotaidis V, Dahmen C, von Plessen G, et al. J Chem Phys 124, 184702, 2006.

[4] Prasad V, Mikhailovsky A, Zasadzinski JA. Langmuir, 21, 7528, 2005.

[5] McLaughlan JR, Roy RA, Ju H, Murray TW. Opt Lett, 35, 2127, 2010.

[6] Lapotko D. Opt Express 17, 2538, 2009.

[7] Lukianova-Hleb EY, Hu Y, Latterini L, et al. ACS Nano 4, 21093, 2010.

[8] Lapotko D, Lukianova K, Shnip A. J Biomed Optics 10, 014006, 2005.

[9] Lukianova-Hleb E, Hanna E, Hafner J, Lapotko D. Nanotechnology 21: 085102, 2010.

[10] Wagner DS, Delk NA, Lukianova-Hleb EY, et al.. Biomaterials 31, 7567, 2010.